Growth Behavior of Anodic Porous Alumina Formed in Malic Acid Solution

Tatsuya Kikuchi*, Tsuyoshi Yamamoto, and Ryosuke O. Suzuki
Faculty of Engineering, Hokkaido University
N13-W8, Kita-ku, Sapporo, Hokkaido, 060-8628, Japan

Abstract

The growth behavior of anodic porous alumina formed on aluminum by anodizing in malic acid solutions was investigated. High-purity aluminum plates were electropolished in CH_3COOH / $HClO_4$ solutions and then anodized in 0.5 M malic acid solutions at 293 K and constant cell voltages of 200 - 350 V. The anodic porous alumina grew on the aluminum substrate at voltages of 200 - 250 V, and a black, burned oxide film was formed at higher voltages. The nanopores of the anodic oxide were only formed at grain boundaries of the aluminum substrate during the initial stage of anodizing, and then the growth region extended to the entire aluminum surface as the anodizing time increased. The anodic porous alumina with several defects was formed by anodizing in malic acid solution at 250 V, and oxide cells were approximately 300 - 800 nm in diameter.

Key words: Aluminum; Anodizing; Porous Alumina; Malic Acid

1. Introduction

Anodic porous alumina is typically obtained by anodizing in acidic solutions. Porous alumina consists of numerous fine hexagonal cells perpendicular to the substrate, and each cell has a nanopore at its center [1-4]. The pores are separated from the aluminum substrate by a thin barrier oxide. Formation of anodic porous alumina is widely performed for the corrosion protection of aluminum and its alloys in aircraft, automobiles, boats, trains, buildings, etc. Recently, the characteristic nanoporous structure has been widely investigated for various applications in the field of micro- and nano-technologies, such as highly ordered templates [5-7], photonic crystals [8, 9], high-density recording media [10, 11], sensors [12], microlens arrays [13, 14], and circuit boards [15].

The structural features of nanoporous alumina can be controlled by the anodizing conditions because the pore interval (cell size) and diameter of the anodic porous alumina are determined by the electrolytes and voltages (electrochemical potential) applied during anodizing [16]. Chromic acid anodizing was patented by Bengough et al. for surface finishing of aluminum and its alloys in 1923 [17]. However, the porous alumina formed in chromic acid solutions is rarely used for nanostructure fabrication because the nanoporous layer has a branching colonial structure [18]. Subsequently, oxalic acid anodizing was also patented by Kujirai et al. in 1923 [19], and highly ordered nanoporous alumina can be obtained by anodizing at constant voltages of 40 V (mild anodizing under low current density) and 120-150 V (hard anodizing under high current density) in this solution [20]. In 1927, sulfuric acid anodizing was patented by Gower et al. [21], and self-ordering voltages were reported at 19-25 V (mild anodizing) and 40-70 V (hard anodizing) [20]. Anodizing in phosphoric and citric acid solutions was reported by Taylor et al. in 1945 [22]. Self-ordered nanoporous alumina can be formed by anodizing in phosphoric acid at 160-195 V, although it is difficult to obtain an ordered nanoporous structure in citric acid due to burning of the anodic oxide [20]. These anodizing electrolytes, oxalic, sulfuric, and phosphoric acids, are widely known as typical self-organized anodizing solutions for nanostructure fabrication.

In the 1970s, Fukushima and co-workers investigated the anodizing behavior of aluminum in various carboxylic acid solutions [23-25]. In that work, they reported that anodic porous alumina could be formed by anodizing in formic, malonic, tartaric, and malic acid solutions, although a porous layer was not obtained in succinic, maleic, fumaric, glutaric, adipic, pimeric, suberic, azelaic, sebacic, lactic, salicylic, resorcylic, acetic, propionic, butyric, valeric, and benzoic acid solutions. In recent years, the nanostructures of porous alumina formed in these organic electrolytes were reported by high-magnification scanning electron microscopy (SEM) [26-28]. Especially, malic acid solution required relatively high voltages of more than 200 V during anodizing, and pore intervals of nanoporous alumina could be achieved in the range of 550 - 950 nm. However, the details of the growth behavior of the nanoporous alumina on the aluminum substrate during anodizing in malic acid solution had not been reported so

far.

In the present investigation, the authors describe the growth behavior of anodic porous alumina formed in malic acid solution, and the nanostructures at each anodizing step are examined. In particular, the formation of the nanoporous layer during the initial stages of anodizing is discussed.

2. Experimental

2.1 Anodizing aluminum in a malic acid solution

Highly pure aluminum plates (99.99 wt%, 110 μm thick, Showa Aluminum Co., Japan, impurities: Fe 10 ppm, Si 9 ppm, and Cu 57ppm) were cut into 20 mm x 20 mm pieces with a handle and then ultrasonically degreased in an ethanol solution for 10 min. After degreasing, the specimens were electropolished in a 13.6 M CH_3COOH / 2.56 M $HClO_4$ solution (T = 280 K) at a constant voltage of 28 V for 60 s to obtain a mirror finished aluminum surface. During electropolishing, an aluminum plate was used as the counter electrode, and the solution was stirred slowly with a magnetic stirrer.

The electropolished specimens were immersed in 0.5 M malic acid solutions (T = 293 K), and then anodized for 48 h at constant voltages of 200 - 350 V to form porous anodic oxide films on the aluminum substrates. During the anodizing, the voltage was increased linearly for the initial 6 min and then was kept to at each corresponding constant voltage with a PC-controlled direct current (DC) power supply (PWR-400H, Kikusui, Japan). A platinum plate was used as the counter electrode and was set 15 mm apart from and parallel to the specimen. The solution was stirred with a magnetic stirrer. After anodizing, the specimens were washed with distilled water and dried in a desiccator.

2.2 Characterization of the anodized specimens

Fig. 1a shows a schematic model of the vertical cross-section of a porous anodic oxide film on aluminum. The nanopores are formed in a disorderly fashion in the anodic oxide during the initial stage of anodizing, and then well-ordered nanopore structures grow at the interface between the anodic oxide and aluminum substrate after a long period of anodizing. Therefore, it is important to observe the interface in addition to the surface of the anodic oxide for an understanding of the growth behavior of anodic porous alumina; the cell arrangement of the porous alumina can be observed on the aluminum substrate. Accordingly, the surface of the aluminum substrate after selective dissolution of the anodic oxide (Fig. 1b) and the bottom of the anodic oxide after selective dissolution of the aluminum substrate (Fig. 1c) were also observed in this investigation.

After anodizing, several anodized specimens were immersed in a 0.20 M CrO_3 / 0.54 M H_3PO_4 solution (T = 353 K) for 30 min to selectively dissolve the anodic oxide film (Fig. 1b), or immersed in a 1.0 M $SnCl_4$ solution (room temperature) for several minutes to selectively dissolve the aluminum substrate (Fig. 1c). The surface morphologies of

the anodized and post-treatment specimens were examined using field emission scanning electron microscopy (FE-SEM, JSM-6500F, JEOL, Japan) and atomic force microscopy (AFM, Nanocute, Hitachi, Japan). The anodized specimens were sputter-coated with platinum using a sputter coater (JFC-1600, JEOL) for SEM observations. To observe their vertical cross-sections, the specimens were embedded in an epoxy resin, mechanically polished, and then immersed in a 0.25 M $K_3[Fe(CN)_6]$ / 4.17 M NaOH solution at room temperature for up to 45 s to clearly observe the nanoporous layer in the anodic oxide. The crystal orientations on the aluminum substrate were measured using electron backscatter diffraction analysis (EBSD, JSM-6500F, JEOL). The elemental distributions on the aluminum specimen were also measured using auger electron spectroscopy (AES, JAMP-9500F, JEOL) and field emission electron probe microanalysis (FE-EPMA, JXA-8530F, JEOL).

3. Results and discussion

3.1 Constant voltage anodizing in malic acid solution and burning phenomena

Fig. 2a shows the changes in the anodic current density, i, with anodizing time, t_a, in a 0.5 M malic acid solution at 293 K and constant cell voltages of V = 200, 250, 300, and 350 V for 66 min. Here, the aluminum specimens were electropolished in a 13.6 M CH_3COOH / 2.56 M $HClO_4$ solution before anodizing, and each anodizing voltage was linearly increased for the first 6 min and then kept at the corresponding constant voltage. For V = 350 V, the current density increased rapidly during the initial voltage increase. Intense gas evolution was observed on the specimen due to the increasing current density. Conversely, the current densities showed steady values of approximately 15 - 25 A m^{-2} for V = 200, 250, and 300 V during the initial voltage sweep. After the initial stage, the current density decreased rapidly to less than 10 A m^{-2} at V = 300 V but then gradually increased to more than 300 A m^{-2}, similar to V = 350 V. Gas evolution was also observed on the anodized specimen after the current density increased. At voltages of 250 and 200 V, the current densities dropped rapidly after the initial 6 min and then showed a steady value of approximately 1 A m^{-2} during anodizing. No gas evolution was observed during this anodizing.

Fig. 2b shows the surface appearance of the anodized specimen at 300 V, current density data for which are shown in Fig. 2a. An anodic oxide film with a gray color was formed on the aluminum, and black oxide regions were also observed on the top and edges of the anodized specimen. These regions are induced by a high current density resulting from the application of a high electric field, and the black anodic oxide films are formed by the local thickening of the anodic oxide. This “burning phenomenon” was already reported previously by Ono et al., where the burned, black oxide films were formed by anodizing under high current density in phosphoric and organic acid electrolytes [27-29]. Oxygen gas evolution occurs at the burned black oxides due to the formation of many defects in the anodic oxide. In contrast, the black anodic oxide was not formed on the specimens during anodizing at 200 and 250 V. To avoid the formation

of burned oxide films, anodizing was carried out at a voltage of 250 V in the following experiments.

Fig. 3 shows the current-time plot curve for long-term anodizing in a 0.5 M malic acid solution at 250 V. The current density showed a small steady value during the initial period of constant voltage anodizing, but the current density increased gradually with anodizing time after 200 min. Then, the current density reached a maximum value of approximately 250 A m^{-2} at 300 min before rapidly decreasing with anodizing time up to 486 min. The current-time plot strongly suggested that the anodic oxide film rapidly grew in the high current density region. Such behavior of the current-time plot is typically measured under the constant voltage anodizing [29]. No burning oxide film was observed on the aluminum specimen after the anodizing. Growth behavior of the nanopores in the anodic oxide will be addressed by SEM observations in the next section.

3.2 Effect of the anodizing time on the formation of anodic porous alumina

Fig. 4a shows an SEM image of the typical surface of a specimen anodized in a 0.5 M malic acid solution at 250 V for 66 min (initial voltage increased for 6 min and constant voltage anodizing applied for 60 min). Here, the stripe pattern observed from the top to bottom on the image corresponds to the rolling marks, which are formed by the rolling process of the aluminum plate. It is noted that numerous narrow white lines were observed on the anodic oxide film. An insert figure shows a high magnification SEM image of the boxed region, and it is clear that the white lines consist of linear self-assembies of nanopores formed on the anodic oxide. The diameter of each nanopore observed on the white lines is approximately 100 - 200 nm. Several fine nanopores were also observed in other regions in addition to the white lines, but the shapes and sizes of these nanopores were unclear. The morphologies of the nanopores over the entire surface of the anodized specimen were also analyzed.

After 66 min of anodizing (Fig. 4a), the specimen was immersed in a 0.20 M CrO_3 / 0.54 M H_3PO_4 solution (T = 353 K) for 30 min to selectively dissolve the anodic oxide film (Fig. 1b). The aluminum substrate obtained after the chemical dissolution of the anodic oxide is shown in Fig. 4b. Numerous white lines approximately 500 nm in width were observed on the aluminum substrate. It is clear from the insert in Fig. 4b that the lines consist of linear self-assemblies of nano-dimples formed on the aluminum substrate by anodizing. In contrast, flat surfaces were observed in the domains separated by each linear assembly, although several nano-dimples were formed on the aluminum substrate. Accordingly, these SEM images suggest that the anodic porous alumina was linearly formed on the aluminum by anodizing in malic acid at 250 V for 66 min.

Fig. 5 shows a) an SEM image and b) a corresponding EBSD analysis map of aluminum substrate obtained by chemical dissolution of the anodic oxide, as shown in Fig. 4. In the EBSD map, the colors show the variations in crystal orientations of the aluminum substrate, and regions with the same color indicate an aluminum grain. The

EBSD map shows that there are several grains with diameters of approximately 10 - 40 μm on the aluminum substrate. By comparing the SEM and EBSD images, the linear assemblies of nano-dimples formed on the aluminum substrate by anodizing correspond clearly to the grain boundaries of the aluminum. Namely, nanopores of the anodic porous alumina are only formed along the grain boundaries in the initial stage of anodizing (low current density region, as shown in Fig. 3). The reason why the nanopores in the anodic oxide are formed at the boundaries will be discussed in the next section.

Fig. 6 shows SEM images of the aluminum substrate of the specimen anodized in a 0.5 M malic acid solution at 250 V for a) t_a = 271, b) 296, and c) 486 min. The anodic oxide was completely dissolved by immersion in a CrO_3/H_3PO_4 solution. During the middle stage of anodizing (t_a = 271 min, Fig. 6a), the current density increased gradually (Fig. 3), and the formation of nano-dimples on the aluminum substrate was extended to near the grain boundaries. In addition, the number of nano-dimples formed on the aluminum grains slightly increased, as seen by comparing Fig. 6a with Fig. 4b. At t_a = 296 min (Fig. 6b), the current density showed a maximum value of 250 A m^{-2} (Fig. 3), and it is clear from the SEM image that there are nano-dimples on the aluminum substrate in the lower half of the image due to the growth of the anodic porous alumina by anodizing for a long time. However, flat regions with no nano-dimples were still present at this stage. During the final stage of anodizing (t_a = 486 min, Fig. 6c), the current density gradually decreased with anodizing time (Fig. 3), and it was found that uniform nano-dimple structures were formed over the entire surface of the aluminum substrate. Therefore, the grain boundaries cannot be differentiated in the figure.

Fig. 7a shows a high-magnification SEM image of the nano-dimple array formed on the aluminum substrate, as shown in Fig. 6c. The nano-dimples, which are approximately 300 - 800 nm in diameter, can be observed over the entire surface of the aluminum substrate. The shape of the nano-dimples was nearly circular, but several dimples had a polygon-like shape. In addition, several white defects were formed at the junction of each nano-dimple. An SEM image of nano-dimple structures was taken from a declined angle, as shown in Fig. 7b. The image shows that fine aluminum pillars with lengths of a few μm were formed at the junction of each nano-dimple, and the aluminum pillars correspond to the white defects in Fig. 7a. These pillars were formed at the fourth and fifth points of the dimple junctions due to the incomplete self-ordering of the anodic porous alumina, but they were not formed at the triple points because of the self-organized cell arrangement.

Fig. 8a shows an SEM image of the bottom surface of the anodic porous alumina formed by anodizing in 0.5 M malic acid solution at 250 V for 486 min. The anodized specimen was immersed in a 1.0 M $SnCl_4$ solution to selectively dissolve the aluminum substrate after anodizing (Fig. 1c). It can be seen that hemispherical nanostructures approximately 300 - 800 nm in diameter are formed, and several black regions are also

observed. These black defects correspond to the positions of the aluminum pillars formed from the incomplete self-ordering of the anodic porous alumina (Fig. 7). An AFM image of the hemispherical nanostructures is shown in Fig. 8b; high-density hemispherical nanostructures with heights of 100 - 300 nm were observed here.

Fig. 9 shows an SEM image of the vertical cross-section of the specimen anodized in a malic acid solution at 250 V for 486 min. Here, the black region at the top corresponds to an epoxy resin, and the gray region at the bottom corresponds to the anodic porous alumina. Stripped patterns were observed in the anodic oxide due to the formation of many nanopores in the anodic porous alumina. However, it is clear that several nanopores in the anodic oxide grew radially. This radial growth may be due to the local growth of the nanopores during the initial stage of anodizing, as described in Fig. 6.

Fig. 10 shows the changes in the current density with anodizing time in a 0.5 M malic acid solution for 2880 min at V = 200, 210, 220, and 230 V. The peak current density for the growth of uniform anodic oxide over the entire surface decreased with anodizing voltage, and the density showed a low value of approximately 2 A m^{-2} at 200 V. In addition, the time before the appearance of the peak current density increased with anodizing voltage. This peak current delay suggests that a long anodizing time is required for the uniform growth of anodic porous alumina. For example, the anodic porous alumina was not formed over the entire surface by anodizing until 1400 min at 200 V. Because the current densities described in Fig. 10 were less than 11 A m^{-2}, the growth rate of the anodic porous alumina was extremely low at this anodizing voltage. On the other hand, the anodizing of aluminum at V = 270 V was also performed in a malic acid solution, but burned anodic oxide was formed on the aluminum substrate by the breakdown of the oxide, as described in Fig. 2a.

3.3 Growth model of anodic porous alumina in malic acid solutions

The current-time plots during anodizing in malic acid solution and SEM images of the oxide and aluminum substrate during each anodizing period are described in Figs. 2 to 10, and the growth behavior of anodic porous alumina will now be discussed. As described in Figs. 2 and 3, current densities of 15 - 25 A m^{-2} were measured during the voltage sweep (6 min) and then remained at low values during anodizing. This current density corresponds to the formation of a thin barrier anodic oxide film, and was already reported by Hoar, et al. [30]. A barrier layer with a dielectric strength of 250 V was formed on the aluminum substrate during this period. After this stage, the current density gradually increased with anodizing time (Fig. 3), and the nanopores were formed along the grain boundaries on aluminum substrate (Fig. 4). Therefore, the current density represents the formation of a nanoporous layer at grain boundaries. The reason why the porous layer was only formed at grain boundaries during this stage may be due to the concentration of impurities at the boundaries. In fact, corrosion and chemical etching of aluminum and its alloys often occur from grain boundaries with elemental impurities. The aluminum plate used in this investigation contains silicon,

iron, and copper impurities (see the experimental section). However, no contaminants were measured at the grain boundaries on aluminum by FE-EPMA and AES analysis due to low levels of these impurities. Further investigation of the porous layer formation at the grain boundaries will be required in the near future.

The formation of anodic porous alumina was extended to regions around the grain boundaries as anodizing time increased (Fig. 6a and 6b). Accordingly, the current density increased gradually with anodizing time (Fig. 3). Therefore, the current density in this stage corresponds to the formation of anodic porous alumina around the grain boundaries. In the final stage, growth of the anodic porous alumina occurred over the entire aluminum surface (Fig. 6c). The current density decreased gradually with increasing anodizing time in this stage. Such current density decreasing during the steady growth of anodic porous alumina was reported during anodizing in other organic acid solutions [29].

In this investigation, the authors could not obtain highly ordered anodic porous alumina fabricated by anodizing in malic acid solution. The self-ordering of anodic porous alumina can be generally achieved at the maximum voltage required to induce high current density anodizing without burning. Therefore, high current density anodizing in malic acid solution at low temperature should be further investigated to avoid burning of the oxide.

4. Conclusions

This investigation showed the growth behavior of the anodic porous alumina formed by anodizing in a malic acid solution under constant applied voltage. Anodic porous alumina can be formed by anodizing in a malic acid solution at less than 250 V, but a black, burned oxide is formed by anodizing in higher electric fields. The porous layer grew at the grain boundaries of the aluminum substrate during the initial stage of anodizing and then completely covered the aluminum surface after anodizing for a long time. Anodic porous alumina with cell diameters of approximately 300 - 800 nm and several defects are formed by anodizing at 250 V.

Acknowledgements

The authors would like to thank Dr. Youngmin Wang (Hokkaido University) for his assistance in the EBSD analysis, Mr. Nobuyuki Miyazaki (Hokkaido University) in the EPMA analysis, and Mr. Keita Suzuki (Hokkaido University) in the AES analysis. This work was financially supported by the Japan Society for the Promotion of Science (JSPS) “KAKENHI”.

References

1) F. Keller, M. S. Hunter, D. L. Robinson, Structural Features of Oxide Coatings on Aluminum, Journal of the Electrochemical Society 100 (1953) 411-419.
2) G. E. Thompson, R. C. Furneaux, G. C. Wood, J. A. Richardson, J. S. Gode,

Nucleation and growth of porous anodic films on aluminium, Nature 272 (1978) 433-435.
3) J. E. Houser, K. R. Hebert, The role of viscous flow of oxide in the growth of self-ordered porous anodic alumina films, Nature Materials 8 (2009) 415-420.
4) K. R. Hebert, S. P. Albu, I. Paramasivam, P. Schmuki, Morphological instability leading to formation of porous anodic oxide films, Nature Materials 11 (2012) 162-166.
5) H. Masuda, K. Fukuda, Ordered metal nanohole arrays made by a two-step replication of honeycomb structures of anodic alumina, Science 268 (1995) 1466-1468.
6) H. Masuda, M. Satoh, Fabrication of gold nanodot array using anodic porous alumina as an evaporation mask, Japanese Journal of Applied Physics 35 (1996) L126-L129.
7) K. Konelius, F. Müller, A.P. Li, U. Göele, Uniform nickel deposition into ordered aluminum pores by pulsed electrodeposition, Advanced Materials 12 (2000) 582-586.
8) H. Masuda, M. Yamada, F. Matsumoto, S. Yokoyama, S. Mashiko, M. Nakao, K. Nishio, Lasing from two-dimensional photonic crystals using anodic porous alumina, Advanced Materials 18 (2006) 213-216.
9) J. Choi, Y. Luo, R.B. Wehrspohn, R. Hillebrand, J. Schilling, U. Göele, Perfect two-dimensional porous alumina photonic crystals with duplex oxide layers, Journal of Applied Physics 94 (2003) 4757-4762.
10) K. Yasui, T. Morikawa, K. Nishio, H. Masuda, Patterned magnetic recording media using anodic porous alumina with single domain hole configurations of 63 nm hole interval, Japanese Journal of Applied Physics 44 (2005) L469-L471.
11) M.T. Rahman, X. Liu, A. Morisako, TbFeCo perpendicular magnetic recording media deposited on nanohole arrays of porous alumina layer, Journal of Applied Physics 99 (2006) 08G9041-08G9043.
12) G. Gorokh, A. Mozalev, D. Solovei, V. Khatko, E. Liobet, X. Correig, Anodic formation of low-aspect-ratio porous alumina films for metal-oxide sensor application, Electrochimica Acta 52 (2006) 1771-1780.
13) T. Kikuchi, Y. Wachi, T. Takahashi, M. Sakairi, R.O. Suzuki, Fabrication of a meniscus microlens array made of anodic alumina by laser irradiation and electrochemical techniques, Electrochimica Acta 94 (2013) 269-276.
14) H. Jha, T. Kikuchi, M. Sakairi, H. Takahashi, Microfabrication of an Anodic Oxide Film by Anodizing Laser-textured Aluminum, Journal of Micromechanics and Microengineering 17 (2007) 1949-1955.
15) H. Jha, T. Kikuchi, M. Sakairi, H. Takahashi, Aluminum Microstructures on Anodic Alumina for Aluminum Wiring Boards, ACS Applied Materials & Interfaces 2 (2010) 774-777.
16) A-P. Li, F. Müller, A. Birner, K. Nielsh, U. Gösele, Polycrystalline nanopore arrays with hexagonal ordering on aluminum, Journal of Vacuum Science & Technology A 17 (1999) 1428-1431.

17) G.D. Bengough, J. M. Stuart, Improved process of protecting surfaces of aluminum and aluminum alloys, UK patent (1923) No. 223994.
18) S. Ono, S. Chiaki, T. Sato, Micro-structure of anodic oxide film on aluminum formed in chromic acid solution, Journal of the Surface Finishing Society of Japan 26 (1975) 456-460.
19) K. Kujirai, S. Ueki, Japan patent (1923) No. 61920.
20) W. Lee, R. Ji, U. Gösele, K. Nielsch, Fast fabrication of long-range ordered porous alumina membranes by hard anodization, Nature Materials 5 (2006) 741-747.
21) C.H.R. Gower, S. O'Brien, Electrolyte containing sulphuric acid, UK patent (1927) No. 290901.
22) C.S. Taylor, C.M. Tucker, J.D. Edwards, Anodic coatings with crystalline structure on aluminum, Journal of the Electrochemical Society 88 (1945) 325-333.
23) T. Fukuchima, Y. Fukuda, G. Ito, Y. Sato, Anodic oxidation and local corrosion of aluminum in mono-carboxylic acids, Journal of the Surface Finishing Society of Japan 21 (1970) 319-326.
24) T. Fukushima, Y. Fukuda, G. Ito, M. Okada, Anodic oxidation of aluminum in aqueous solutions of dicarboxylic acids, Journal of the Surface Finishing Society of Japan 25 (1974) 447-452.
25) T. Fukushima, Y. Fukuda, G. Ito, M. Miyoshi, Anodic oxidation of aluminum at high current density in the aqueous solution of hydroxycarboxylic acids, Journal of the Surface Finishing Society of Japan 25 (1974) 537-541.
26) S.Z. Chu, K. Wada, S. Inoue, M. Isogai, Y. Katsuta, A. Yasumori, Large-scale fabrication of ordered nanoporous alumina films with arbitrary pore intervals by critical-potential anodization, Journal of the Electrochemical Society 153 (2006) B384-B391.
27) S. Ono, M. Saito, M. Ishiguro, H. Asoh, Controllong factor of self-ordering of anodic porous alumina, Journal of the Electrochemical Society 151 (2004) B473-B478.
28) S. Ono, M. Saito, H. Asoh, Self-ordering of anodic porous alumina induced by local current concentration: Burning, Electrochemical and Solid-State Letters 7 (2004) B21- B24.
29) S. Ono, M. Saito, H. Asoh, Self-ordering of anodic porous alumina formed in organic acid electrolytes, Electrochimica Acta, 51 (2005) 827-833.
30) T.P. Hoar, J. Yahalom, The initiation of pores in anodic oxide films formed on aluminum in acid solutions, Journal of the Electrochemical Society, 110 (1963) 614-621.

Captions

Fig. 1 Schematic models of a) anodic porous alumina, b) the aluminum substrate formed by selective dissolution of the anodic oxide, and c) the anodic oxide formed by selective dissolution of the aluminum substrate.

Fig. 2 a) Changes in current density, i, with anodizing time, t_a, in 0.5 M malic acid solutions (293 K) at constant voltages of V = 200, 250, 300, and 350 V for 486 min. Before anodizing, the specimens were electropolished in 13.6 M CH_3COOH / 2.56 M $HClO_4$ solution (280 K) at a constant voltage of 28 V for 60 s. b) Surface appearance of a specimen anodized at 300 V.

Fig. 3 Change in current density, i, with anodizing time, t_a, in a 0.5 M malic acid solution (293 K) at 250 V for 486 min.

Fig. 4 SEM images of the anodized specimen a) before and b) after anodic oxide removal in a 0.20 M CrO_3 / 0.54 M H_3PO_4 solution (T = 353 K) for 30 min. High-magnification SEM images are also shown in each figure. The specimen was anodized in a 0.5 M malic acid solution (293 K) at 250 V for 66 min.

Fig. 5 a) SEM image and b) EBSD orientation map of the aluminum substrate obtained by anodizing at 250 V for 66 min and anodic oxide removal. Conditions of the oxide removal are as in Fig. 4. The EBSD map shows crystallographic orientation of the aluminum substrate.

Fig. 6 SEM images of the aluminum substrate obtained by anodizing at 250 V for a) t_a = 271, b) 296, and c) 486 min and anodic oxide removal.

Fig. 7 High-magnification SEM images of the aluminum substrate obtained by anodizing at 250 V for 486 min and anodic oxide removal.

Fig. 8 a) SEM and b) AFM images of the bottom surface of the anodic porous alumina formed by aluminum substrate removal a 1.0 M $SnCl_4$ solution. The anodizing conditions are same as Fig. 7.

Fig. 9 SEM image of the cross-section of a specimen anodized at 250 V for 486 min in a 0.5 M malic acid solution.

Fig. 10 Changes in current density, i, with anodizing time, t_a, in 0.5 M malic acid solutions (293 K) at constant voltages of V = 200, 210, 320, and 230 V for 1440 min.

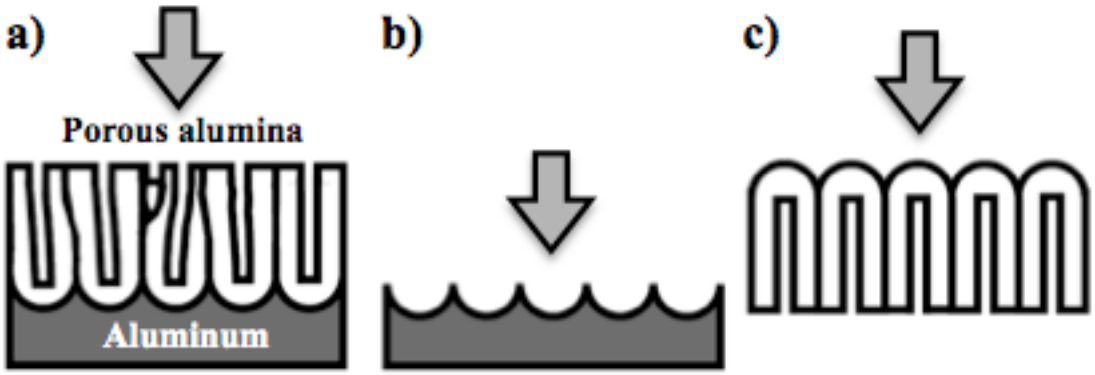

Fig. 1

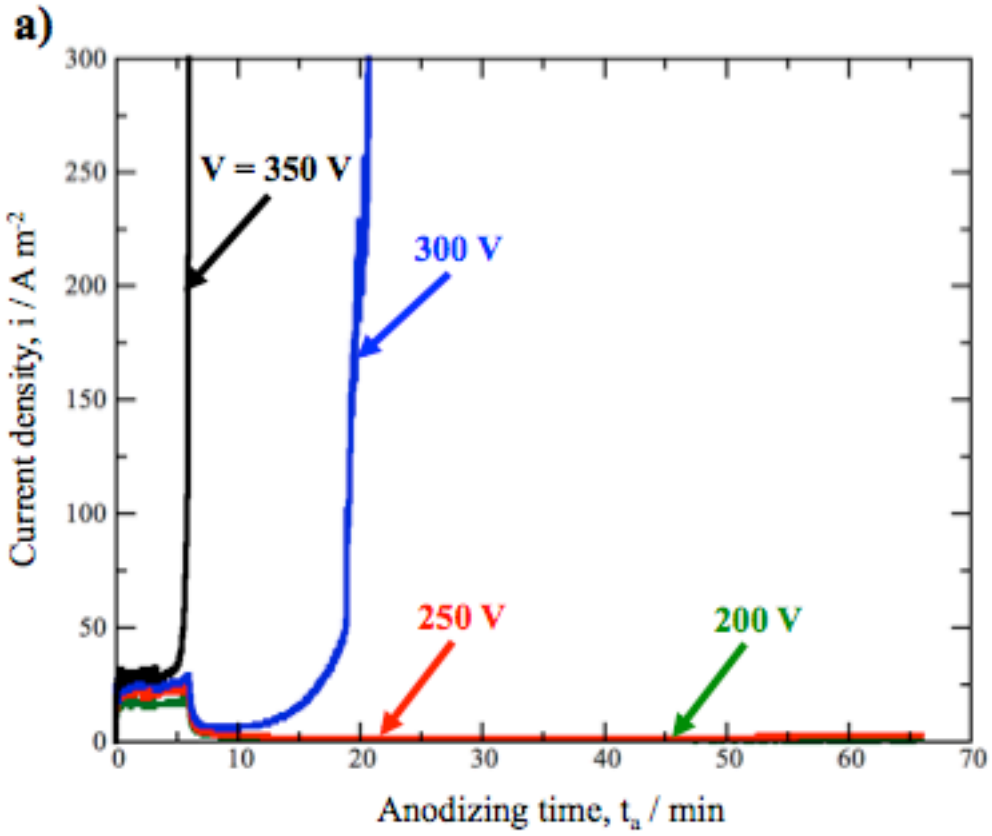
a)
Current density, i / A m-2
Anodizing time, ta / min
V = 350 V
300 V
250 V
200 V
0
50
100
150
200
250
300
0
10
20
30
40
50
60
70

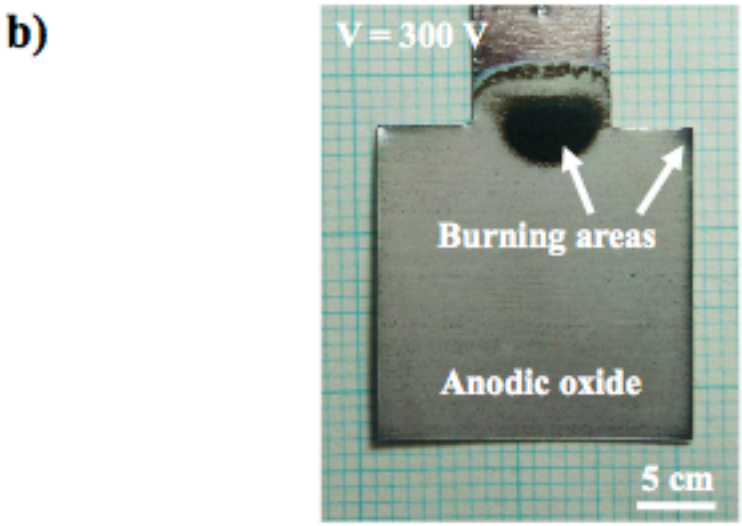
b)
V = 300 V
Burning areas
Anodic oxide
5 cm

Fig. 2

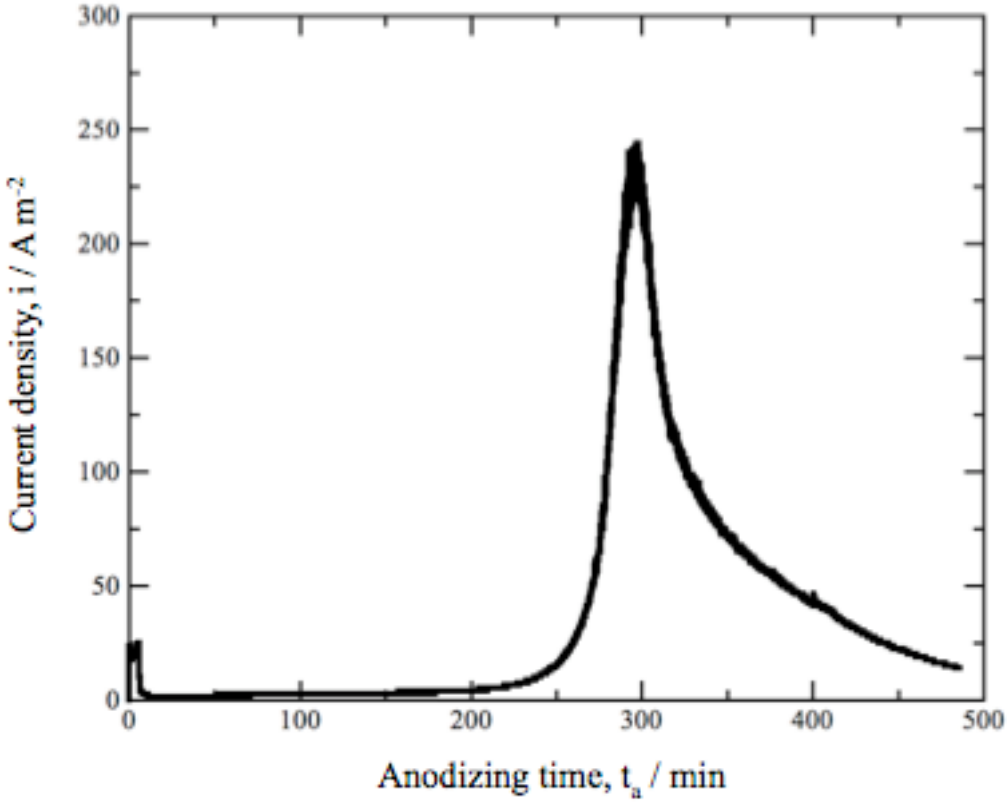
Current density, i / A m^{-2}
300
250
200
150
100
50
0
0
100
200
300
400
500
Anodizing time, t_a / min

Fig. 3

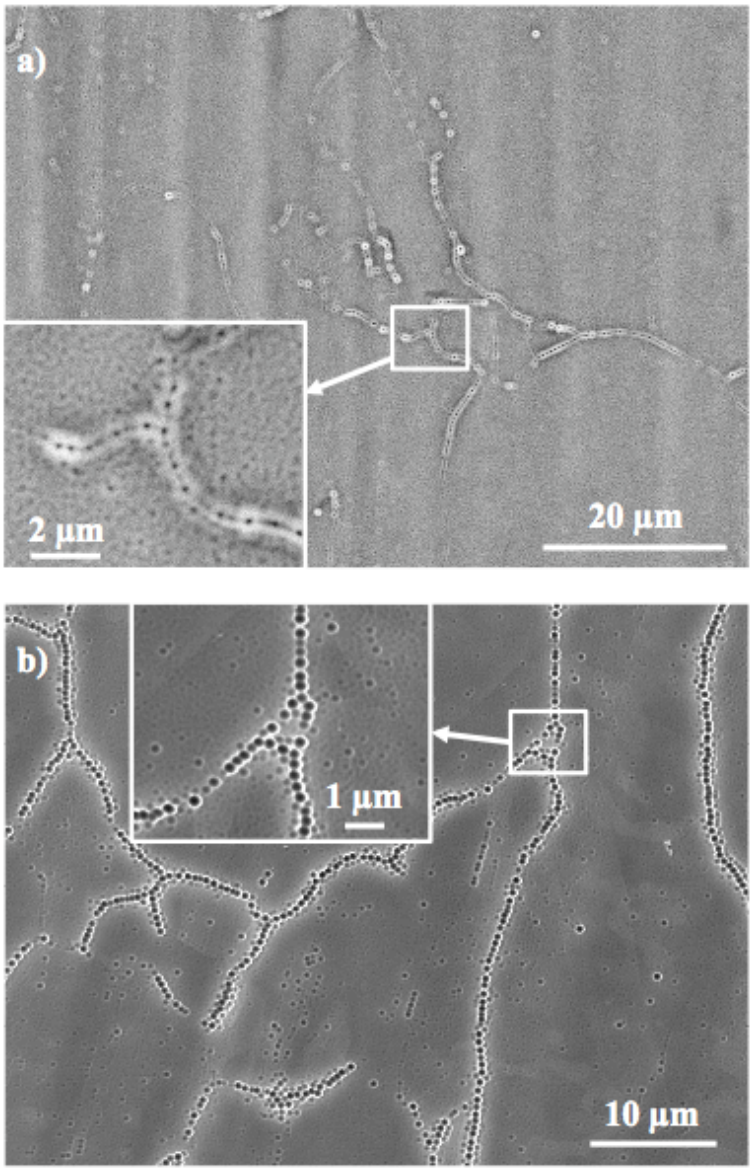

Fig. 4

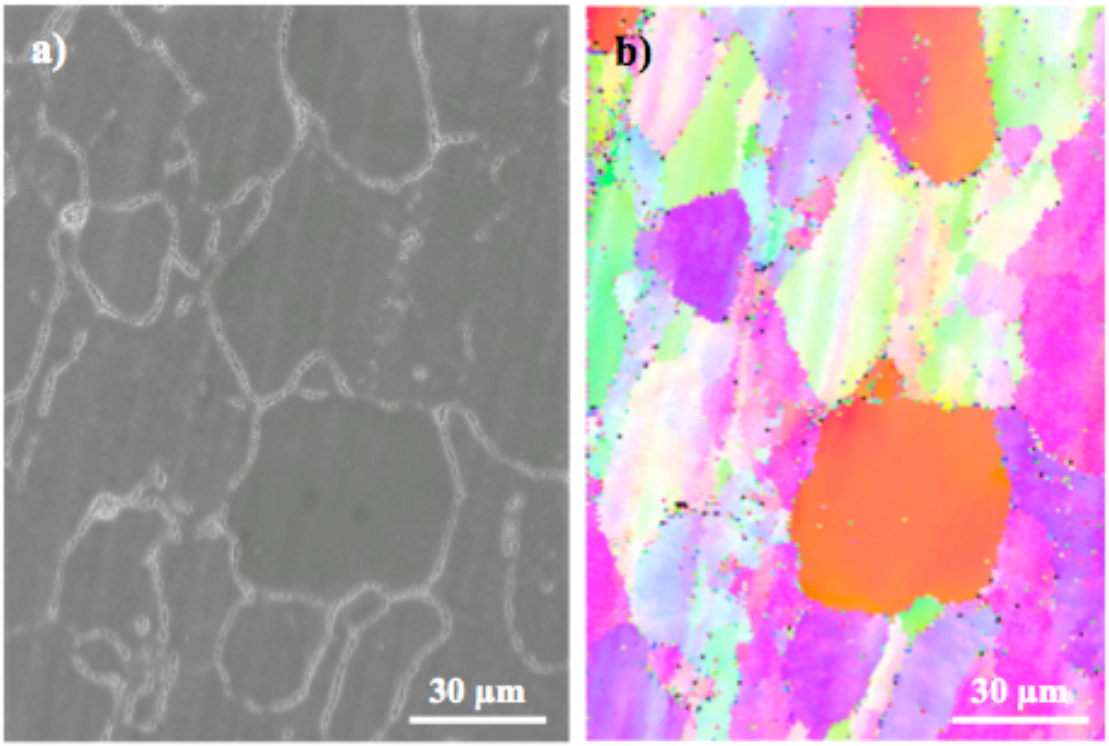

Fig. 5

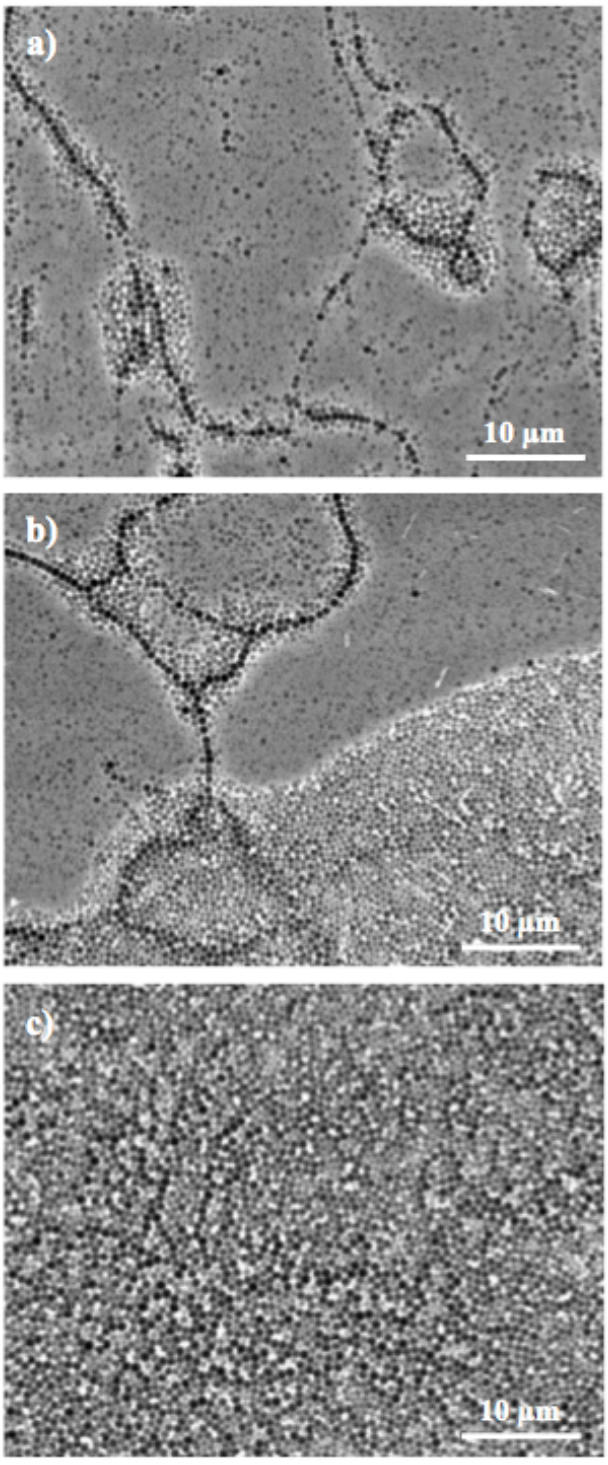

Fig. 6

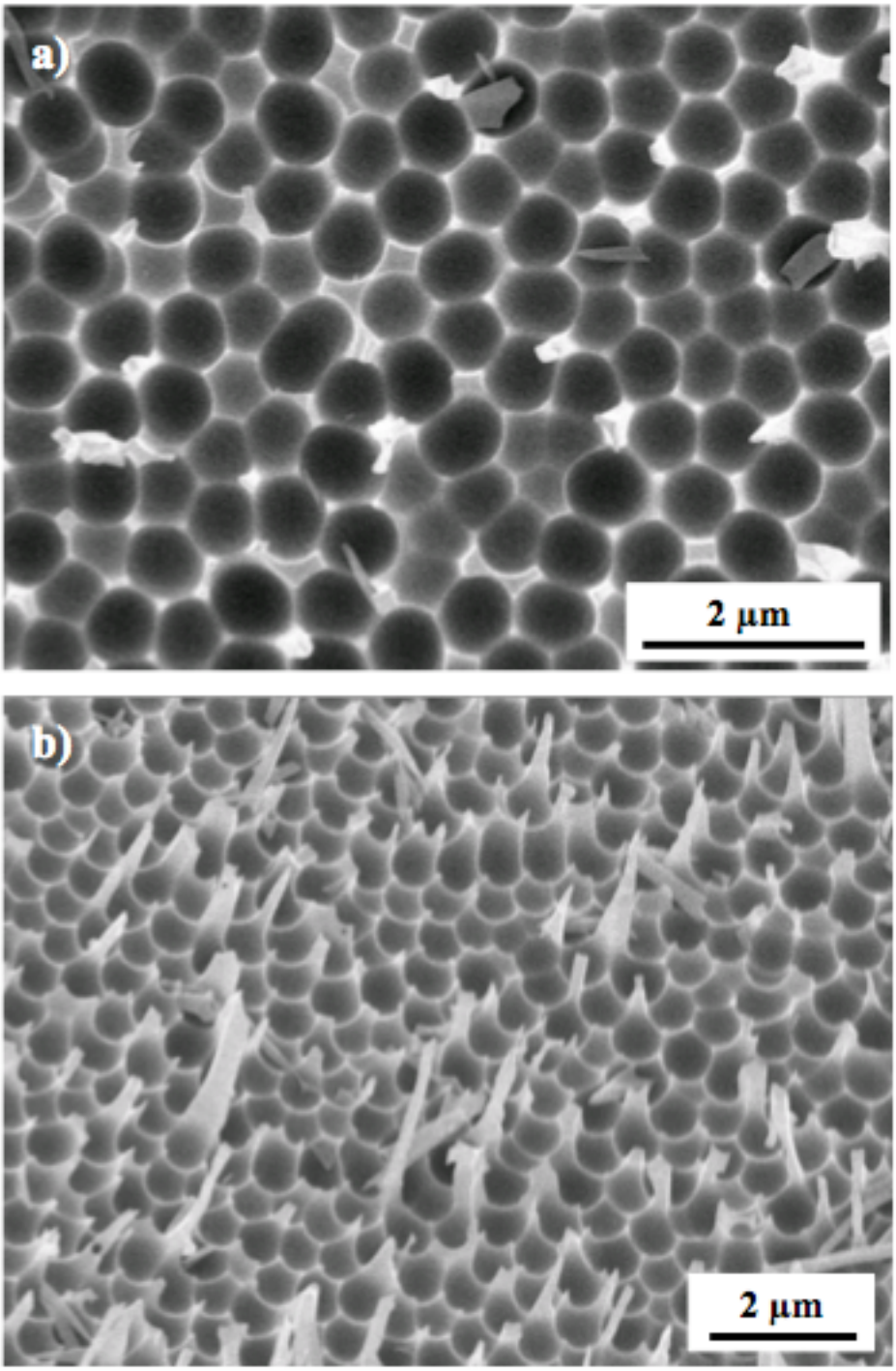

Fig. 7

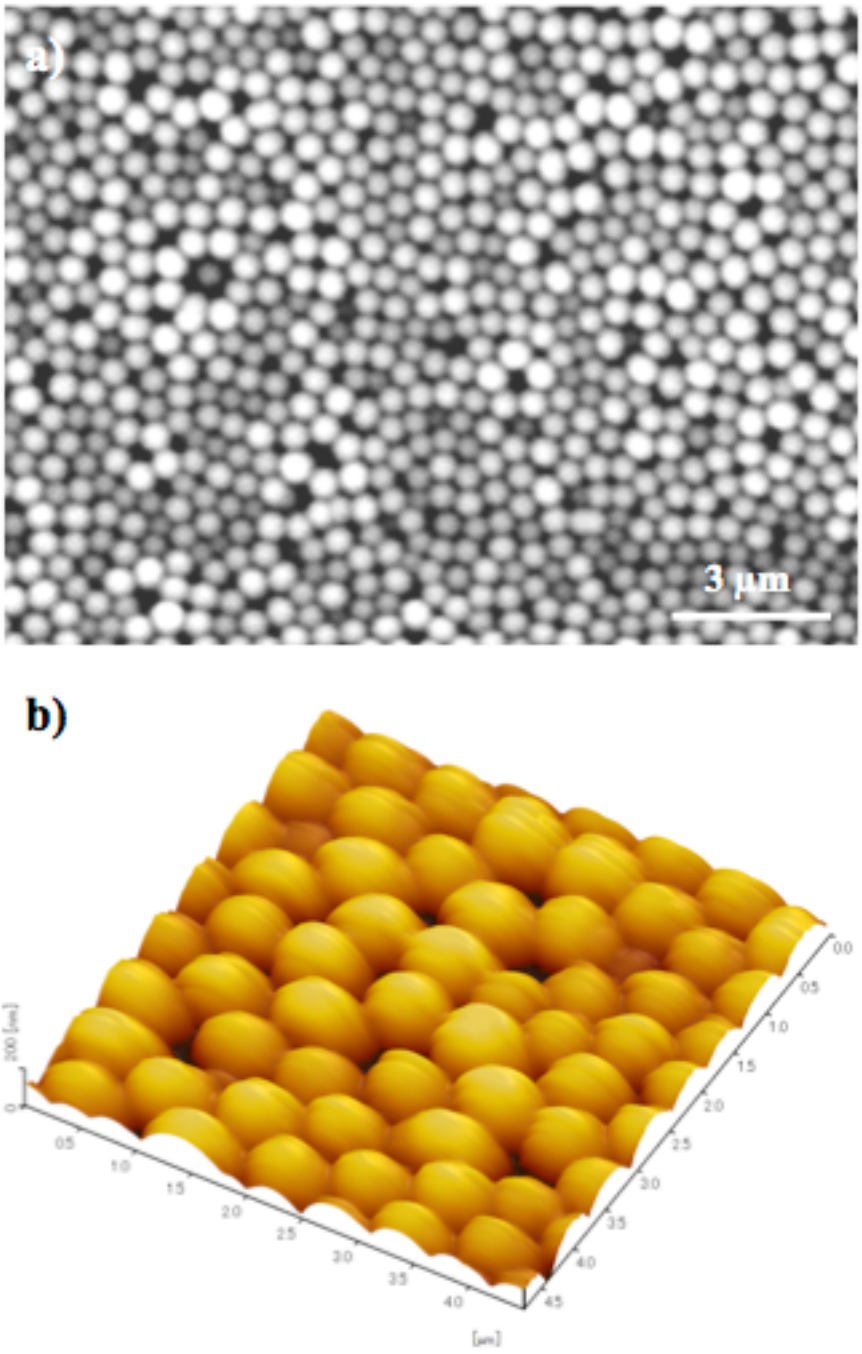
a)
3 µm
b)
200 [nm]
0
0.5
1.0
1.5
2.0
2.5
3.0
3.5
4.0
4.5
[µm]
0.0
0.5
1.0
1.5
2.0
2.5
3.0
3.5
4.0
4.5

Fig. 8

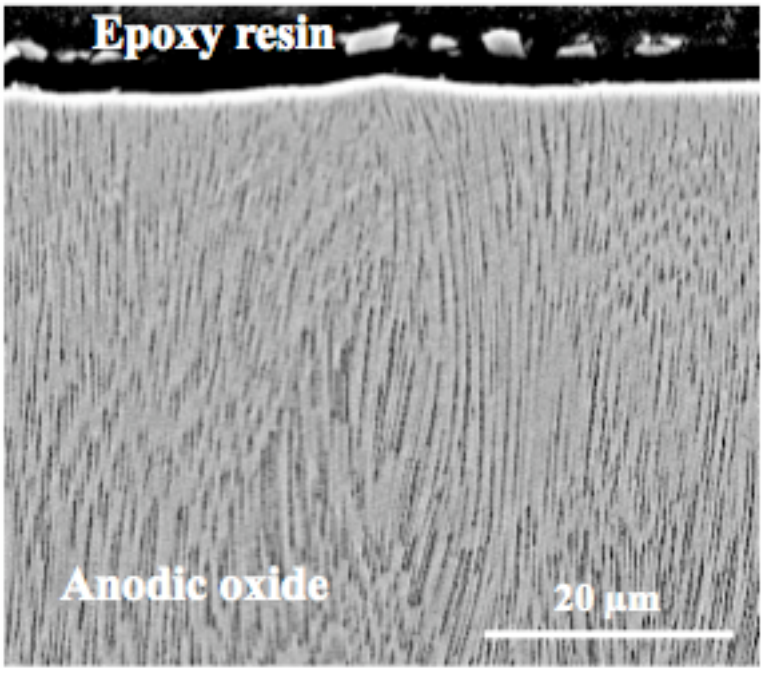

Fig. 9

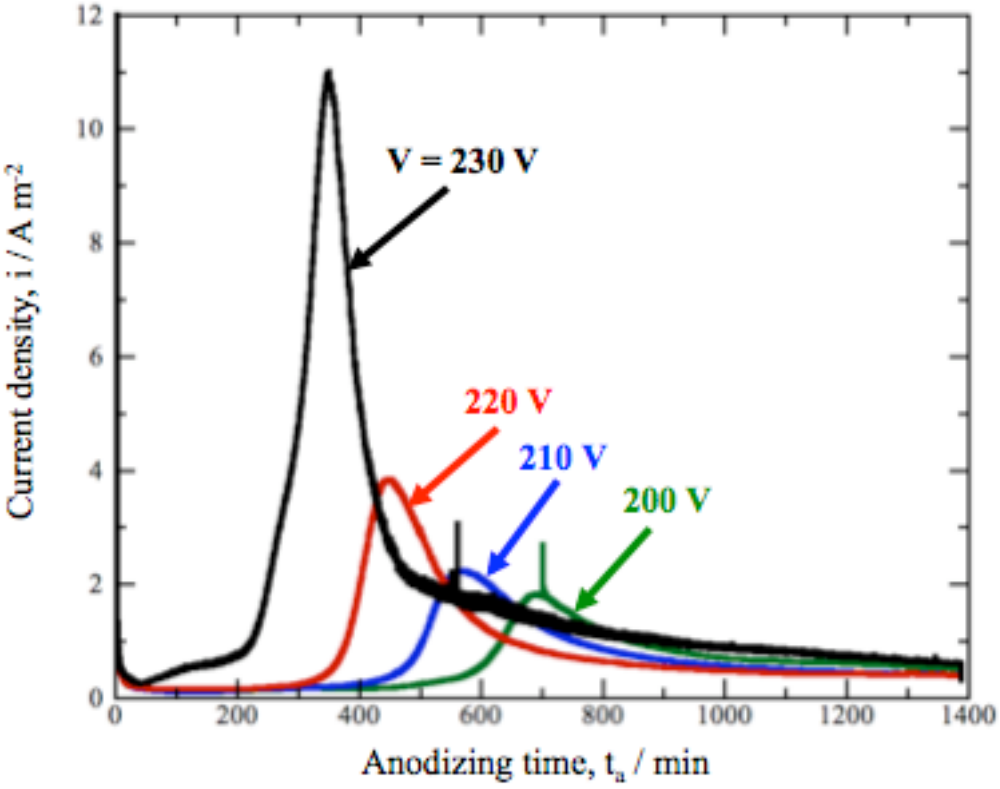
Current density, i / A m-2
Anodizing time, ta / min
V = 230 V
220 V
210 V
200 V
0
2
4
6
8
10
12
0
200
400
600
800
1000
1200
1400

Fig. 10